POLITEHNICA UNIVERSITY OF BUCHAREST

Doctoral School of Electronics, Telecommunications and Information Technology

Decision no. ____ from __-__-____

Ph.D. THESIS SUMMARY

Ing. Cristina Adelaida HEIMAN

TEHNICI DE TRANSFORMARE A POLARIZĂRII PENTRU ANTENE DIRECTIVE

POLARIZATION TRANSFORMING TECHNIQUES FOR DIRECTIVE ANTENNAS

THESIS COMMITTEE

Prof. Dr. Ing. Ion MARGHESCU Univ. Politehnica din București	President
Prof. Dr. Ing. Răzvan TAMAȘ Univ. Politehnica din București	PhD Supervisor
Prof. Dr. Ing. Tudor PALADE Univ. Tehnică din Cluj-Napoca	Referee
Conf. Dr. Ing. Alin DĂNIȘOR Univ. Maritimă din Constanța	Referee
Prof. Dr. Ing. Teodor PETRESCU Univ. Politehnica din București	Referee

BUCHAREST 2023

Contents

Chapter 1

Introduction

In space communications, ensuring the highest possible signal-to-noise ratio is one of the most important aspects considering the long distances at which such radio links are made, but also the low powers of the transmitters located on the space vehicle. For this reason, antennas with high directivity are used in most applications, among which horn antennas are the most common.

Another challenge in designing antennas for such applications is to ensure circular polarization, as the upper layers of the atmosphere cause the polarization of radio waves to rotate.

1.1 Presentation of the PhD domain

Space communications refers to both radio links between a spacecraft (satellite, orbital space station, transport spacecraft) and a ground station, and communications between two spacecraft (between two satellites in a constellation). These communications refer both to the transmission of information in both directions, but also to command-and-control signals.

A separate category of applications is constituted by the systems for the automatic orientation of the ground station antenna in the direction of the space vehicle with which the radio communication is carried out.

Most directional antennas for space communications are in the form of one or more horn antennas, sometimes equipped with a parabolic reflector. Ensuring a circular polarization, necessary to respond to the polarization rotation of radio waves when passing through the ionosphere, can be achieved either by intervening in the transmission medium that excites the horn antenna (usually a waveguide), or by placing in the antenna aperture elements that produce polarization rotation.

1.2 Purpose of the PhD work

The aim of the work is the development of methods that allow changing the polarization of directional antennas (pyramidal horn type), without interfering in the excitation system of the antenna. Compared to the solution proposed in most approaches of specialized literature, which assume the introduction of a polarizer (for example, a diaphragm provided with a slot) inside the waveguide that excites the antenna, in this

work is being investigated the possibility of obtaining polarization rotation through the placement of multilayered periodic structures in the aperture of a pyramidal horn antenna.

After a theoretical analysis of the methods that allow polarization rotation, several configurations of such periodic structures are analyzed and compared, both by simulation and by experimental determinations.

1.3 Dissertation content

The PhD thesis begins with a theoretical chapter (Chapter 2) in which the types of horn antennas used in space communications and the methods of designing a pyramidal horn antenna excited by a waveguide are presented. A case study is presented in which a pyramidal horn antenna is characterized for the Ku band. The case study consists in designing the horn antenna structure and validating the results through simulation and experimental determinations.

In chapter 3, the analysis of a double ridged guide horn antenna, with linear polarization, with excitation through a transmission line is proposed. The component elements of the antenna are dimensioned, and then the whole assembly is analyzed for different types of dielectrics with the maximum relative permittivity of 2.2 between the two ridges inside the horn antenna.

In the fourth chapter, the characteristics of propagation through the ionosphere in space communications are presented, namely the characterization of the ionosphere, the refractive index, the variability of the total electron content, the estimation of the effects of the total electron content on the propagation in the measurement of a radio source and the polarization rotation when passing through ionosphere.

A method of transforming the polarization of a pyramidal horn antenna using slots in the excitation guide is presented in chapter 5. The general principle of the method consists in introducing a diaphragm with a slot inside the horn antenna's excitation guide.

A new method of transforming the polarization of a pyramidal horn antenna is presented in chapter 6. The method consists in obtaining a dual polarization with the help of a linear radiator inclined to the direction of the incident electric field. The polarization change is achieved by adding some multilayer types of frequency selective surface structures in the horn aperture.

In order to validate the pyramidal horn antenna with frequency selective surfaces in the horn aperture, simulations were performed using software tools (development environments such as ANSYS HFSS, MATLAB, Inventor) and experimental determinations using the radiating systems characterization platform from the Constanța Maritime University.

Chapter 7 presents the conclusions of the PhD thesis, the original contributions, the list of works published during the advanced research program and the prospects for further development of research on the subject addressed. Personal contributions to the optimization and improvement of a conventional pyramidal horn antenna to achieve circular polarization are presented.

Chapter 2

Waveguide excited pyramidal horn antennas

2.1 E-plane sectoral horn antenna

2.1.1 The fields produced at the aperture

The fields at the aperture horn are given by [1]:

$$E_z' = E_x' = H_y' = 0, \tag{2.1a}$$

$$E_y'(x', y') \simeq E_1 cos\left(\frac{\pi}{a}x'\right) e^{-j[ky'^2/(2\rho_1)]}, \tag{2.1b}$$

$$H_z'(x', y') \simeq jE_1\left(\frac{\pi}{ka\eta}\right) sin\left(\frac{\pi}{a}x'\right) e^{-j[ky'^2/(2\rho_1)]}, \tag{2.1c}$$

$$H_x'(x', y') \simeq -\frac{E_1}{\eta} cos\left(\frac{\pi}{a}x'\right) e^{-j[ky'^2/(2\rho_1)]}, \tag{2.1d}$$

2.1.2 Radiated fields

Components of the electric field radiated by the horn in the E-plane and in the H-plane:

E-plane ($\phi = \pi/2$)

$$E_r = E_\phi = 0, \tag{2.43}$$

$$E_\theta = -j\frac{a\sqrt{\pi k\rho_1}E_1 e^{-jkr}}{8r}\left\{-e^{j\left(\frac{k\rho_1 sin^2\theta}{2}\right)}\left(\frac{2}{\pi}\right)^2 (1+\cos\theta)F(t_1', t_2')\right\}, \tag{2.44}$$

$$t_1' = \sqrt{\frac{k}{\pi\rho_1}}\left(-\frac{b_1}{2} - \rho_1 \sin\theta\right), \tag{2.45}$$

$$t_2' = \sqrt{\frac{k}{\pi\rho_1}}\left(+\frac{b_1}{2} - \rho_1 \sin\theta\right). \tag{2.46}$$

H-plane ($\phi = 0°$)

$$E_r = E_\theta = 0 \tag{2.47}$$

$$E_{\phi} = -j\frac{a\sqrt{\pi k\rho_1}E_1 e^{-jkr}}{8r}\left\{(1+\cos\theta)\left[\frac{\cos\left(\frac{ka}{2}\sin\theta\right)}{\left(\frac{ka}{2}\sin\theta\right)^2-\left(\frac{\pi}{2}\right)^2}\right]F(t_1'', t_2'')\right\}, \quad (2.48)$$

$$t_1'' = -\frac{b_1}{2}\sqrt{\frac{k}{\pi\rho_1}}, \quad (2.49)$$

$$t_2'' = +\frac{b_1}{2}\sqrt{\frac{k}{\pi\rho_1}}. \quad (2.50)$$

2.1.3 Directivity

Horn directivity in E-plane:

$$D_E = \frac{4\pi U_{max}}{P_{rad}} = \frac{64a\rho_1}{\pi\lambda b_1}|F(t)|^2 = \frac{64a\rho_1}{\pi\lambda b_1}\left[C^2\left(\frac{b_1}{\sqrt{2\lambda\rho_1}}\right)+S^2\left(\frac{b_1}{\sqrt{2\lambda\rho_1}}\right)\right]. \quad (2.67)$$

2.2 Aperture matched horns

Introducing curved sections at the edges does not eliminate diffractions, but replaces edge diffractions with curved surface diffractions. Compared to conventional horn, this radiation mechanism leads to smoother patterns with reduced side lobes and negligible reflections back into the horn.

2.3 Multimode horns

A multimode horn is the diagonal horn, the electric field lines in the cross section consist of a superposition of TE_{10} and TE_{01} modes in a square waveguide. Another type of multimode horn where the apertures reduced side lobes, equal main lobe apertures, and cross-polarization is the dual-mode conical horn.

2.4 Phase center

Each far-zone field component radiated by an antenna can be written, in general, as:

$$E_u = \hat{u}E(\theta,\phi)e^{j\psi(\theta,\phi)}\frac{e^{-jkr}}{r} \quad (2.74)$$

where $\hat{u}$ is a unit vector.

The reference point that makes $\psi(\theta,\phi)$ independent of θ and ϕ is known as the phase center of the antenna. When referenced to the phase center, the antenna produces spherical waves.

2.5 Case study: characterization of a pyramidal horn antenna for Ku band

2.5.1 The design of the pyramidal horn antenna

Determining the dimensions of a horn antenna depends on the gain (20 dBi), the transverse dimensions of the waveguide a and b and the length of the waveguide L, so the dimensions are 15.7 mm, 9.4 mm and 31 mm respectively.

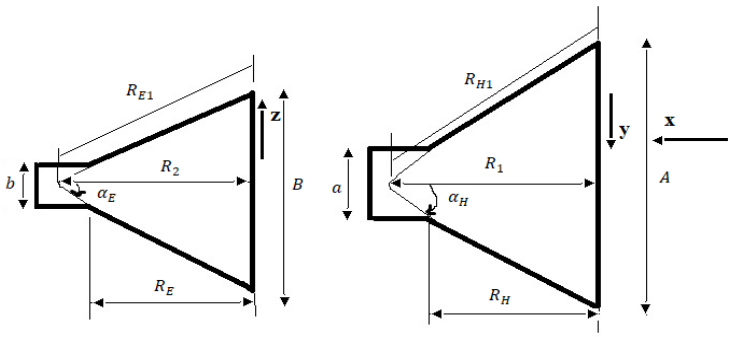

(a) (b)

Figure 2. 1 *Aperture geometry in the E-plane (a) and in the H-plane (b) of the horn antenna along the Oz axis (in the direction of propagation)*

Next, the remaining dimensions will be determined to obtain the desired gain $(A, B, \alpha_e, \alpha_h, R_E, R_H)$ (Figure 2. 1) [1]. The dimensions of the aperture in the direction of E-plane and H-plane are $A = \sqrt{3\lambda R_1}$ and $B = \sqrt{2\lambda R_2}$. The height of the pyramidal horn is given by [1]:

$$R_E = (B - b)\left[\left(\frac{R_{E1}}{B}\right)^2 - \frac{1}{4}\right]^{\frac{1}{2}}, \tag{2.79}$$

$$R_H = (A - a)\left[\left(\frac{R_{H1}}{A}\right)^2 - \frac{1}{4}\right]^{\frac{1}{2}}, \tag{2.80}$$

The remaining dimensions of the antenna are related to the parameters:

$$R_2{}^2 = R_{E1}{}^2 - \left(\frac{B}{2}\right)^2 = R_{E1}{}^2 - \left(\frac{\sqrt{2\lambda R_2}}{2}\right)^2, \tag{2.82}$$

$$R_1{}^2 = R_{H1}{}^2 - \left(\frac{A}{2}\right)^2 = R_{H1}{}^2 - \left(\frac{\sqrt{3\lambda R_1}}{2}\right)^2, \tag{2.83}$$

$$\alpha_E = tan^{-1}\frac{B}{2R_2}, \tag{2.84}$$

$$\alpha_H = tan^{-1}\frac{A}{2R_1}, \tag{2.85}$$

The iterative approach led to six possible parameter values, so all antennas were simulated, the best results are obtained for antenna 3.

2.5.2 Antenna characterization through simulations and measurements

The antenna has been optimized for the 13.3 GHz frequency. $|S_{11}|$ as a function of frequency is shown in Figure 2.24. The measurement results are also included in the graph for comparison.

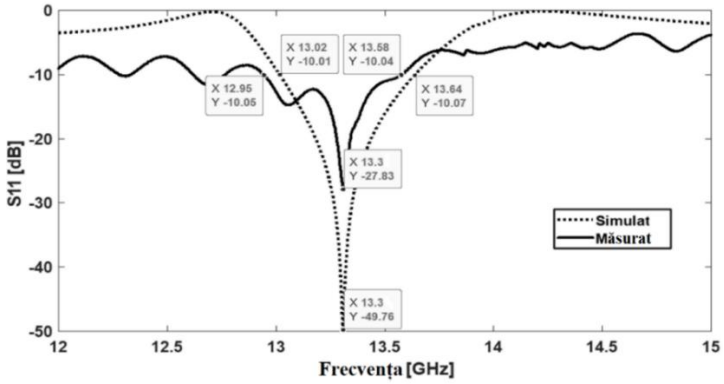

Figure 2.24 *$|S_{11}|$ depending on the frequency*

In the main radiation direction, the simulated gain is 21.36 dB, and the measured one is 21.88 dB, see Figure 2.29. From the experimental results it was concluded that the polarization of the proposed horn antenna is linear.

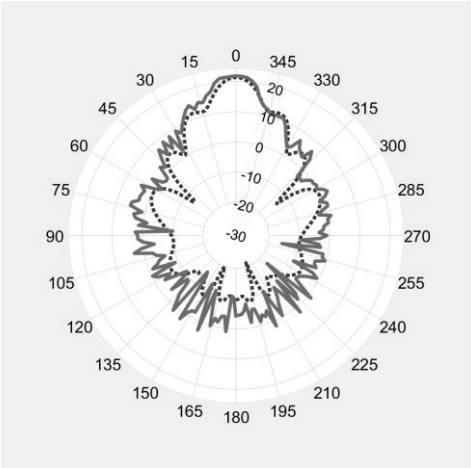

Figure 2.29 *Variation of radiation pattern with elevation angle at the frequency of 13.3 GHz in the E-plane (simulated values are represented by dotted line and measured values are represented by solid line)*

2.5.3 Study of an array of two horn antennas

In this paragraph, the results of an array simulations consisting of two horn antennas of the previously described type are presented. The antenna array was excited by a Wilkinson circuit to share the same power to the two antennas and then an impedance matching circuit was designed. Compared to the case of a single antenna, in the case of a string consisting of two antennas, an increase in the gain, but also in the reflection coefficient, is observed.

Chapter 3

Double ridged guide horn antennas with excitation through transmission line

3.1 The design of the double ridged guide horn antennas

3.1.1 The structure of the horn antenna

The double ridged guide horn antenna comprises three areas: the excitation area, the double waveguide, and the aperture.

3.1.2. Waveguide design

The cross-section of the double ridged waveguide is shown in Figure 3.4.

The cutoff frequency of the rectangular ridged waveguide is [2]:

$$f_c' = \frac{1}{\pi\sqrt{\mu\varepsilon}\sqrt{\left(\frac{s}{d}+\frac{2C_d}{\varepsilon}\right)(a-s)b}}, \tag{3.2}$$

When the frequency tends to infinity, the wave impedance of the dominant mode (TE_{10}) can be calculated as [2]:

$$Z_{0\infty} = \frac{120\pi}{\frac{2C_d}{\varepsilon}cos\left(\frac{s\lambda_c}{a\lambda_c'}\right)\frac{\pi}{2}+\frac{1\lambda_c'}{\pi\, d}\left(sin\left(\frac{s\lambda_c\pi}{a\lambda_c'^2}\right)+\frac{d}{b}cos\left(\frac{s\lambda_c\pi}{a\lambda_c'^2}\right)tg\left(\left(1-\frac{s}{a}\right)\frac{\lambda_c\pi}{\lambda_c'^2}\right)/2\right)}. \tag{3.7}$$

The wave impedance at frequency can be calculated as follows [2]:

$$Z_0 = Z_{0\infty}/\sqrt{1-\left(\frac{f_c'}{f}\right)^2}. \tag{3.8}$$

The dimensions of the ridged waveguide are as follows: a = 27 mm, b = 16 mm, s = 10 mm and d = 5,55 mm.

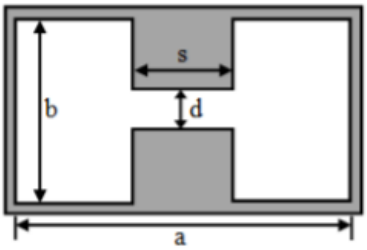

Figure 3.4 *Cross section of double ridged waveguide structure*

3.1.3. Ridged design

The dimensions of the horn aperture are 109.5 mm × 90.84 mm, with an axial length of 118.65 mm. The ridge was constructed from two parts: one with linear variation and the other with exponential variation. The exponential variation [3] is of the form:

$$y(z) = qe^{uz}\,, \tag{3.9}$$

where u is an independent variable and q is determined from the total length of the exponential ridge.

3.1.4. Horn design

The dimensions of the horn are calculated on the same principle presented in section 2.5.2. The pyramidal horn was designed at 12 GHz with a gain of 20 dB and the transverse dimensions of the waveguide are $a = 27$ mm and $b = 16$ mm. Thus, the aperture dimensions are $A = \sqrt{3\lambda R_1} = 109{,}5$ mm, $B = \sqrt{2\lambda R_2} = 90{,}84$ mm, $R_{E1} = 151{,}7$ mm, $R_{H1} = 166{,}1$ mm, $R_2 = 165{,}04$ mm and $R_1 = 160$ mm. The lengths of the horn in the two planes are: $R_E = 118{,}65$ mm and $R_H = 118{,}65$ mm. Since the R_E and R_H values are equal, it can be concluded that the design parameters that are selected for the antenna are correct to produce a gain of 20 dB.

3.2 Antenna characterization through simulations

3.2.1 Double ridged guide horn antenna with Rogers type dielectric

The double ridged guide horn antenna has good Ku-band performance by adding a dielectric between the two ridges (Figure 3.1). In Figure 3.2 $|S_{11}|$ is represented and an improvement can be seen over the dielectric-free double ridged guide horn antenna.

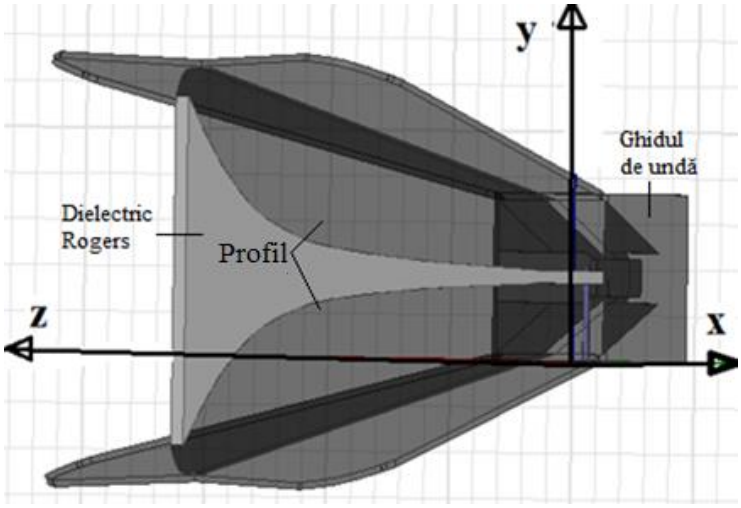

Figure 3.1 *Double ridged guide horn antenna with dielectric between the two ridges*

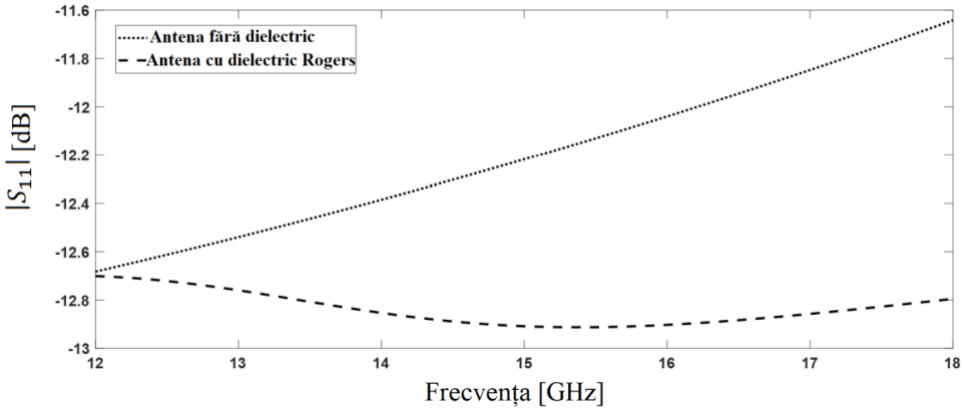

Figure 3.2 *The reflection coefficient for the horn antenna without dielectric, respectively with Rogers type dielectric*

3.2.2 Double ridged guide horn antenna with Teflon type dielectric

In this case, a better reflection coefficient is obtained when using a Rogers-type dielectric between the two ridges than using a Teflon-type dielectric.

Chapter 4

Characteristics of ionospheric propagation in space communications

4.1 Characterization of the ionosphere

Absorption of solar radiation decreases with altitude. This is explained by the fact that ionization is much lower while increasing height [4]:

$$N_e(h) = N_e(h_m)e^{(k[1-Z-e^{-Z}])} = N_e e^{1-Z-sec\chi e^{-Z}} \quad , \tag{4.1}$$

where h_m is the height at maximum density $N_e(h_m)$. If q_0 is the maximum ion generation rate ($m^{-3}s^{-1}$) and α recombination rate (m^3s^{-1}), the maximum density is given by $N_e(h_m) = \sqrt{\frac{q_0}{\alpha_{rec}}}$. Parameter χ eliminates the dependence of the solar elevation angle on the Chapman layer and k represent the two distinct formulations of processes in the ionosphere: α-Chapman (k = 0,5) and β-Chapman (k = 1).

4.2 Refractive index of the ionosphere and total electron content (TEC)

The electromagnetic wave passing through the ionosphere is characterized by the Appleton-Hartree equation [4]:

$$n^2 = \frac{X}{1-jZ-\left(\frac{Y_T^2}{2(1-X-jZ)}\right)\pm\left(\frac{Y_T^4}{4(1-X-jZ)^2+Y_L^2}\right)^{\frac{1}{2}}} \quad , \tag{4.7}$$

where n is the complex refractive index, X represents the thermal motion of electrons, Y_L represents the Lorentz force due to the interaction of electrons with the magnetic field, Y_T is the transverse component of the Lorentz force.

If the collision frequency is negligible, equation (4.7) becomes:

$$n^2 = 1 - \frac{2X(1-X)}{2(1-X)-Y^2sin^2\theta \pm [Y^4sin^4\theta + 4Y^2cos^2\theta(1-X)^2]^{\frac{1}{2}}} . \quad (4.13)$$

At frequencies much higher than the electron/ion gyroscopic frequency, equation (4.13) reduces to:

$$n^2 \approx 1 - X = 1 - \frac{f_p^2}{f^2} \ , \quad (4.14)$$

where f_p is the plasma frequency and f is the propagation frequency of electromagnetic waves propagating through the plasma.

4.3 Variability of total electron content

Observations of the ionosphere on smaller time scales reveal transient variations. The cause of spatial and temporal variations has been linked to numerous physical processes [4].

4.3.1 TEC variability

The variability is caused by the movements of atmospheric layers and plasma dynamics under the action of electrodynamic processes. Atmospheric gravitational waves and strong electric fields give rise to plasma density gradients which in turn cause electron density instabilities manifested as TEC variations.

4.3.2 Calculation of TEC variability at a given frequency

Calculate the TEC along the propagation path (I_{P_φ}):

$$I_{P_\varphi} = \frac{1}{2}\frac{f_1^2}{40.308}[(P_1 - L_1\lambda_1) + K + aLP], \quad (4.21)$$

where f_1 is the frequency of the signal from the satellite of a navigation system, P_1 is the additional radio propagation path, L_1 is the number of phase rotations at the signal frequency, λ_1 is the wavelength, K is determined by the ambiguity of the phase measurements and the propagation time of the signal and aLP represents the influence of noise on phase and group delay measurements at the carrier frequency.

Then, the elevation and azimuth angles of the satellites are calculated, and the data series are separated into continuous time intervals. To estimate the TEC along the propagation path, I_M is:

$$I_M = S_j^i I_V(\phi, l, t) + I_{K,j} \ , \quad (4.22)$$

where ϕ is the latitude of the point of intersection of the direction between the receiving satellite and the ionosphere, at a height of 450 km, l is the longitude of this point, I_V is the value TEC, I_K is a constant defined for every continuous interval and S_j^i is the oblique factor.

4.4 Estimating the effects of total electron content on radio wave propagation

A method for estimating the effects of ionospheric disturbances is presented. Differential phase parameter measurements are simulated, and GPS observations are used to calculate the slant TEC (sTEC) and phase value [4].

Distance calculated using GPS-type measurements for the pseudocode P_c is related to the actual distance ρ so:

$$P_c = \rho + \delta\rho^{ion} + \delta\rho^{trop} + c(\delta t_c^S - \delta t_c^R) + c(b^S + b^R) + \Delta\,, \qquad (4.28)$$

where $\delta\rho^{ion}$ and $\delta\rho^{trop}$ are the errors due to ionospheric and tropospheric delays, δt_c^S and δt_c^R are the clock errors between the satellite and the receiver, b^S and b^R are the offset errors between the satellite and the receiver, Δ is the error due to inter-path interference, satellite phase center offsets (frequency dependent) as well as random errors.

4.5 Polarization rotation in the ionosphere

The received signal undergoes changes [4], fluctuations when propagating through the ionosphere, thus a phenomenon called depolarization occurs caused by the rotation of the polarization plane of electromagnetic wave oscillations when passing through ionized media (Faraday effect) and through structures containing water or ice particles. A solution to the depolarization problem is to use two circularly polarized waves in opposite directions.

4.5.1. Linear polarization

Vertical polarization is obtained when the electric field has a vertical direction to the direction of propagation of the electromagnetic wave. In contrast, horizontal polarization is obtained when the electric field is horizontal to the direction of propagation.

4.5.2. Circular polarization

A harmonic time-varying wave is circularly polarized if at a given point in space the electric (or magnetic) field vector describes a circle as a function of time. The field vector (electric or magnetic) must meet the following conditions: the field must have two orthogonal components with linear polarization, the two components must have the same amplitude and have a phase difference odd multiples of 90°.

Chapter 5

Polarization transformation of a pyramidal horn antenna using slots in the excitation guide

5.1 Waveguide and slot design

The structure of the pyramidal horn antenna with circular polarization is presented in Figure 5.1.

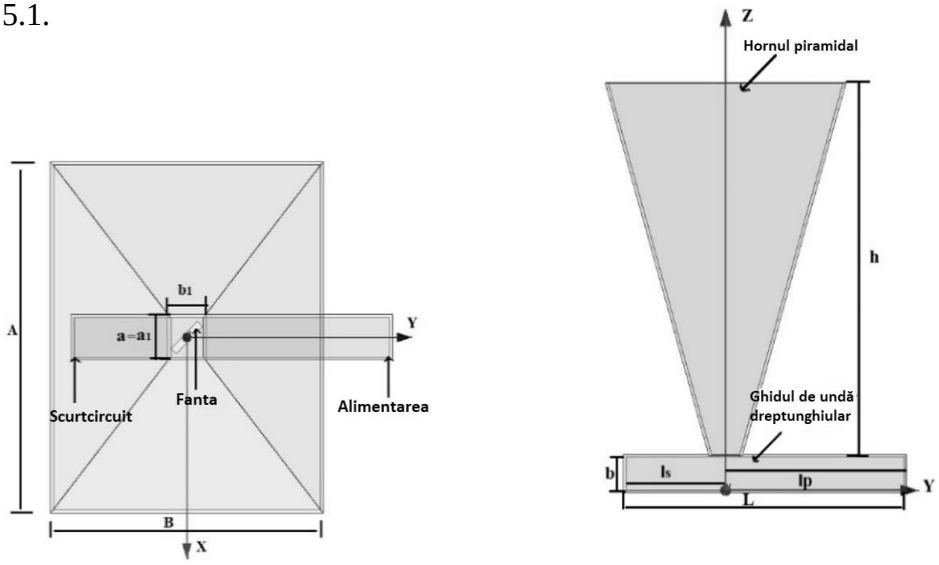

(a) (b)

Figure 5.1 *Horn antenna dimensions: top view (a) and side view (b)*

5.1.1 Rectangular waveguide

The wavelength in the guide is calculated according to the following equation [5]:

$$\lambda_g = \frac{\lambda_0}{\sqrt{1-\left(\frac{\lambda_0}{\lambda_c}\right)^2}} \tag{5.1}$$

where λ_c is the critical wavelength and λ_0 is the wavelength in free space.

The phase shift constant β for TE_{mn} mode is expressed by [5] in:

$$\beta = \sqrt{(2\pi/\lambda_0)^2 - (m\pi/a)^2 - (n\pi/b)^2} \tag{5.2}$$

Depending on the length of the waveguide (L), different phase shifts between them may occur 90° [5]:

$$\beta_1 L - \beta_2 L = \pi/2 \tag{5.3}$$

where β_1 represents the phase shift constant of the TE_{10} mode and β_2 represents the phase shift constant of the TE_{01} mode.

The transverse dimensions and length of the rectangular waveguide are: $a =$ 12,23 mm, $b = 11{,}9$ mm and $L = 102{,}65$ mm.

5.1.2 Slot made in the sidewall of the waveguide

The components of the normalized field for the mode of propagation TE_{10} are [6]:

$$H_z = j \cos\frac{\pi x}{a} e^{j(\omega t - \beta_{10} z)} \tag{5.4}$$

$$H_x = \frac{-\beta_{10}}{\pi/a} \sin\frac{\pi x}{a} e^{j(\omega t - \beta_{10} z)} \tag{5.5}$$

$$E_y = \frac{\omega \mu_0}{\pi/a} \sin\frac{\pi x}{a} e^{j(\omega t - \beta_{10} z)} \tag{5.6}$$

To achieve circular polarization, the slot must be inserted on the top of the wall of the rectangular waveguide with an inclination of 45°. Thus, the dimensions of the slot are: $l_s = 0{,}53\lambda_g$, $l_p = 0{,}95\lambda_g$, slot width of $0{,}1\lambda_0$ and slot length of $0{,}52\lambda_0$.

5.2 The design of the horn antenna

In the pyramidal horn, TE_{10} and TE_{01} modes are excited through the waveguide, the total field in the aperture is given by [6]:

$$\begin{cases} E_s = \hat{y} E_y^{10} + \hat{x} j E_x^{01} \\ H_s = -\frac{\hat{x} E_y^{10}}{Z_0} + \frac{\hat{y} j E_x^{01}}{Z_0} \end{cases} \tag{5.7}$$

Pyramidal horn dimensions can be calculated with the optimal pyramidal horn design equation [7] knowing the gain (G = 20 dB), operating frequency (f = 13 GHz) and dimensions at the base of the horn (a_1 and b_1). Thus, the dimensions at the base of the horn are $a_1 = a = 12{,}23$ mm and $b_1 = 10{,}5$ mm, and the dimensions of the aperture in the two planes are $A = 107{,}4$ mm, $B = 87$ mm and $h = 134$ mm.

5.3 Antenna characterization through simulations

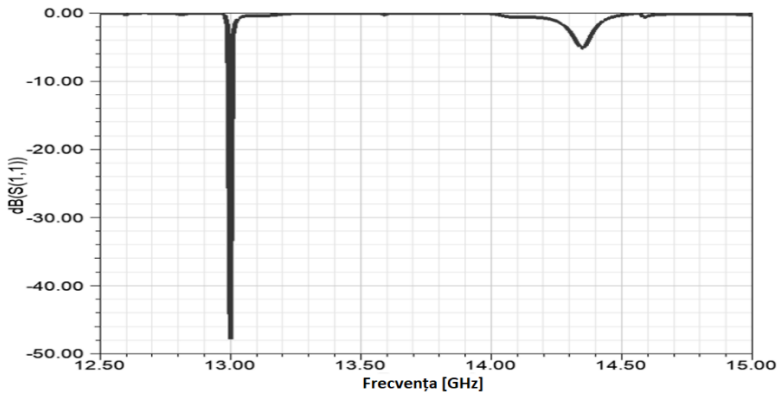

Figure 5.8 *Simulation of parameter S_{11} as a function of frequency*

$|S_{11}|$ from Figure 5.8 for the frequency of 13 GHz is of – 47 dB. The difference between the two types of polarization is about 9 dB, which is a good thing because this type of antenna was made to have a right hand circular polarization.

Chapter 6

Polarization transformation of a pyramidal horn antenna using frequency selective surface structures

An alternative way of transforming the polarization of the antenna is presented, basically by adding several layers of frequency selective surfaces in front of the aperture of the pyramidal horn. Frequency Selective Surfaces (FSS) are much simpler and consist of half-wavelength tilted linear dipoles. Compared to other multilayer structures, the FSS layers have been spaced so that they operate on the principle of a Yagi-Uda antenna array.

6.1 Frequency selective surfaces

The term frequency selective surface refers to a multitude of resonant structures that interact at certain frequencies with unguided electromagnetic radiation [8]. FSS are usually composed of a multitude of identical elements called unit cells, with which the electromagnetic wave interacts [9]. A unit cell is made up of conducting and insulating materials.

6.1.1 Types of FSS and their applications

The first application is a structure called the Salisbury screen, which represented one of the first frequency selective surface concepts. The second application is to integrate such an FSS in a device called a radome to protect antennas against atmospheric agents [10], [11]. Other applications involve a direct integration of a frequency selective surface into an antenna.

6.1.2 FSS unit cell geometry

In the specialized literature, there are a multitude of geometries used for FSS cells, but the metallic cross-type element is one of the most widespread. There are metal band [9], square patch [10], circular patch [11], ring [12], square loop [13] or Jerusalem cross [17] shaped structures.

6.1.3 Multilayer frequency selective surfaces

Several applications where multilayer FSSs appear are described. In the first application, an FSS-based polarization converter is placed in the aperture of a standard antenna [18], the second application features an active FSS [16], and the third application presents a circular polarizer with beamforming characteristics based on FSS [17].

6.2 Transforming wave polarization by using arrays of passive radiators

6.2.1 Generating a dual polarization using a linear radiator tilted with respect to the distance of the incident electric field

Consider a TEM wave propagating along the O_z axis. The electric field intensity vector is:

$$\mathbf{E} = E_x(z,t)\hat{a}_x + E_y(z,t)\hat{a}_y, \tag{6.1}$$

$$E_x(z,t) = E_{x,0}\cos(\omega t - k_0 z), \tag{6.2}$$

$$E_y(z,t) = E_{y,0}\cos(\omega t - k_0 z + \Delta\Phi), \tag{6.3}$$

where $k_0 = \frac{2\pi}{\lambda}$ and $\Delta\Phi$ is the initial phase shift between the two components of the electric field.

If $\Delta\Phi = \frac{\pi}{2}$ and additionally, $E_{x,0}$=$E_{y,0}$=E_0 then:

$$\mathbf{E} = E_0\left[\hat{a}_x\cos(\omega t - k_0 z) + \hat{a}_y\sin(\omega t - k_0 z)\right]. \tag{6.6}$$

In this case, $\mathbf{E} =$ ct, and the polarization of the wave is circular.

Surface current density induced on the surface of the radiator:

$$\mathbf{J}_s = \frac{2}{\sqrt{2}}\hat{n} \times \mathbf{H}_i, \tag{6.7}$$

where $\hat{n}$ is the direction of the normal to the surface of the conductor.

The induced current can be found by integrating the current density on the side surface of the radiator:

$$I = 2\pi a\frac{2H_i}{\sqrt{2}} = 4\pi a\frac{E_i}{Z_0\sqrt{2}}, \tag{6.8}$$

where Z_0 is the free space wave impedance.

The components of the total electric field (incident and reradiated) are:

$$E_{x,tot} = -E_{rx} = jk_0E_i\frac{a}{2r}\exp(-jk_0r)\mathrm{d}s', \tag{6.11}$$

$$E_{y,tot} = E_i + E_{ry} = \frac{E_i}{2r}(2r_0 - jk_0\mathrm{d}s'a)\exp(-jk_0r), \tag{6.12}$$

where r_0 is the distance between the primary radiation source and the elementary dipole.

When $r_0 \gg a$, the first term in his expression $E_{y,tot}$ is dominant, and $E_{x,tot}$ and $E_{y,tot}$ will be out of phase with each other by approximately $\pi/2$.

6.2.2 FSS unit cells potentially usable as polarization transformers

Four types of unit cells were analyzed and simulations were performed for different widths of the resonant element in the range of 1.5 mm and 3 mm with the step of 0.5 mm.

6.3 Converting a pyramidal horn antenna into a circularly polarized antenna

6.3.1 Analysis of the original pyramidal horn antenna

Departed from an existing horn antenna (Figure 6.14 (a)), for the X band (8÷12 GHz). The transverse dimensions of the waveguide are $a = 22{,}86$ mm and $b = 10{,}16$ mm, and the length is 90 mm. A is 81 mm, B is 61 mm, the height of the horn is 86 mm, the length of the monopole is 7,5 mm, the radius is 0,76 mm, and its position relative to the short circuit wall is 11,5 mm.

The simulated gain is 10.6 dBi and the measured gain is 9.22 dBi (Figure 6.). $|S_{11}|$ is below –11 dB over the entire frequency band, both for measured and simulated figures.

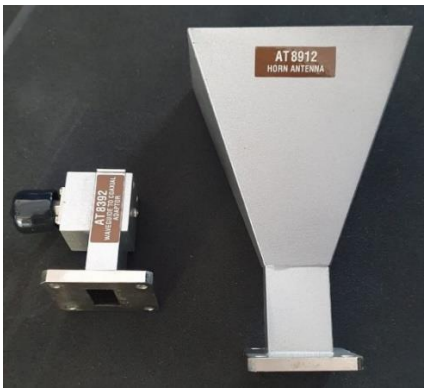

(a)

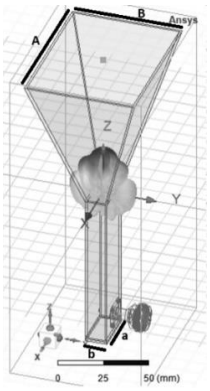

(b)

Figure 6.14 *Pyramidal horn antenna: AT8912 horn antenna (a) and antenna model in Ansoft HFSS program*

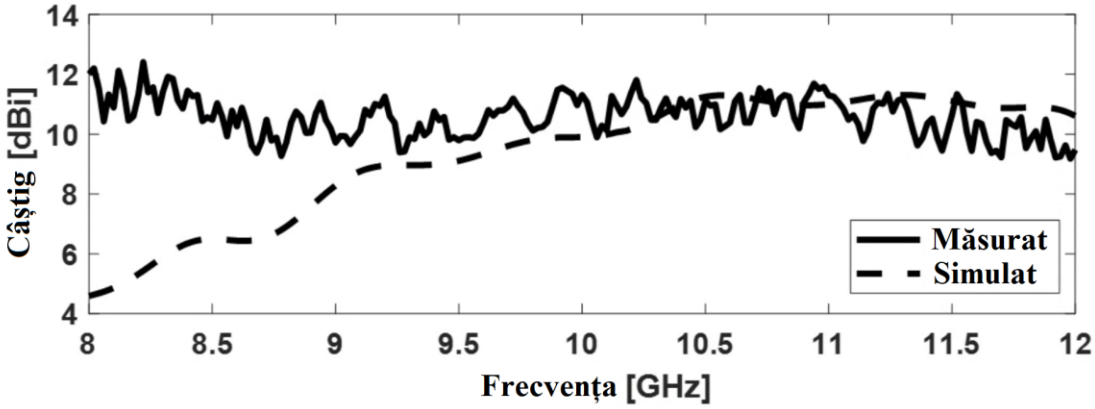

Figure 6.16 *Gain of the pyramidal horn antenna in the main direction of radiation*

6.3.2 Radiating systems with circular polarization consisting of a horn antenna and FSS layers

The first stage consisted in determining the optimal number of elements of an FSS layer, this study being carried out for cross-shaped radiators (+). The second stage aimed at establishing the optimal number of FSS layers and optimizing the shape of the radiating elements.

6.3.2.1 FSS structure with N × N cross-shaped elements

The system is operating on the principle of a Yagi-Uda antenna system consisting of λ/2 dipole antennas. In the opening of the pyramidal horn, the FSS structure with the cross-type radiators (+), rotated at an angle of 45°, was added in front of the pyramidal horn aperture. Following the performance analysis of the assembly consisting of the horn antenna and FSS structures, it turned out that the best option is the FSS structure with 4 × 4 resonant elements.

6.3.2.2 Multiple layer FSS structures

The distances between successive layers are calculated using a dedicated online calculator. The FSS structure consists of 4 × 4 radiators. Three types of FSS structures are made, varying the width of the radiators, but also the number of layers of FSS structures placed in front of the aperture of the pyramidal horn.

The variants considered to be the best were chosen according to the performances offered, regarding the axial ratio and the difference between the gain for

cross-polarization and co-polarization, respectively. Figure 6.22 shows the physical FSS structures for each selected version.

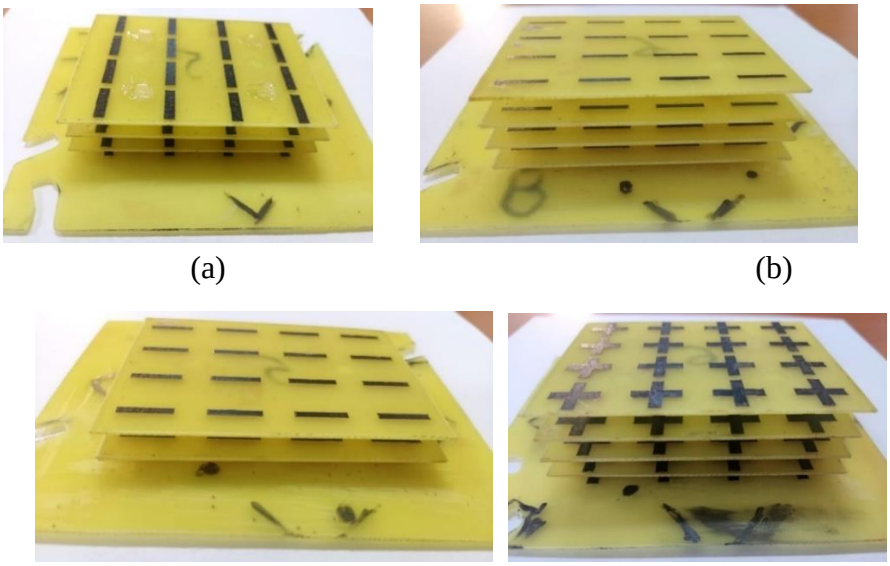

(a) (b)

(c) (d)

Figure 6.22 *Three-dimensional view of the fabricated FSS structures for the chosen variants 5 – (a), 1 – (b), 2 – (c) and 8 – (d)*

6.3.3 Antenna characterization through simulations and measurements

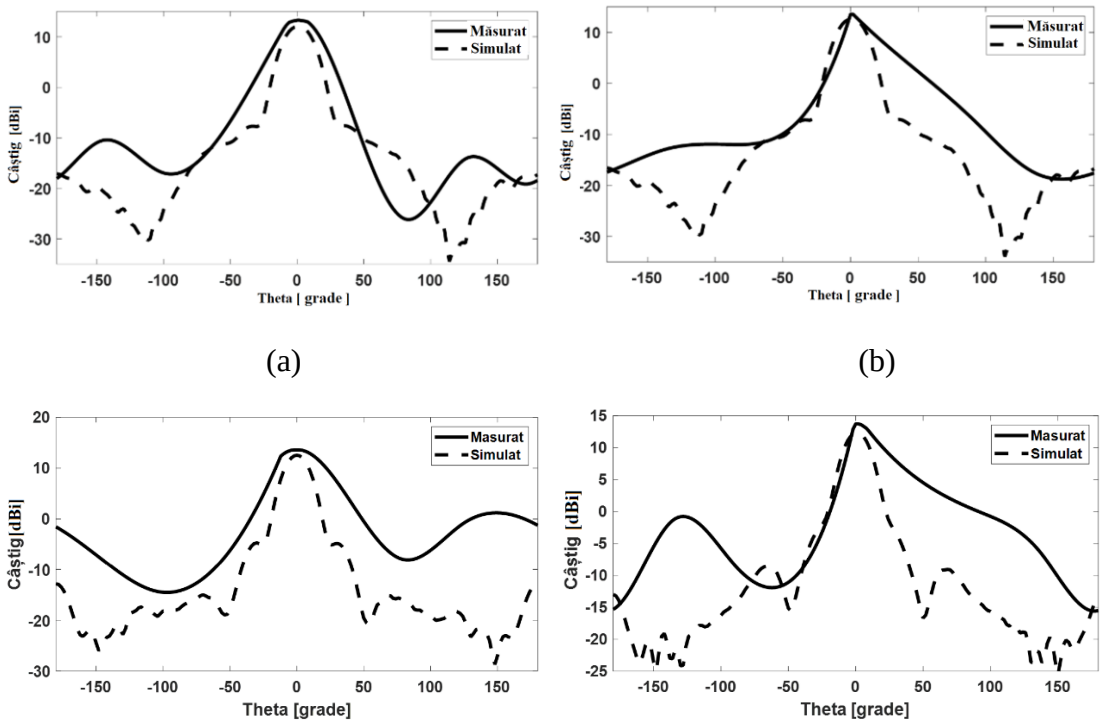

(a) (b)

(c) (d)

Figure 6.30 *Variation of the radiation pattern with the elevation angle at the frequency of 12 GHz in the H-plane for the four variants of the frequency selective surface*

The variation of $|S_{11}|$ with the frequency for the four FSS-horn structures is below -11 dB over the entire frequency band in simulations, and below -5 dB in measurements.

Figure 6.30 shows a comparison between the radiation pattern of our radiating system resulting both from simulation and measurements at 12 GHz frequency. Figure 6.38 shows the axial ratio for each individual configuration.

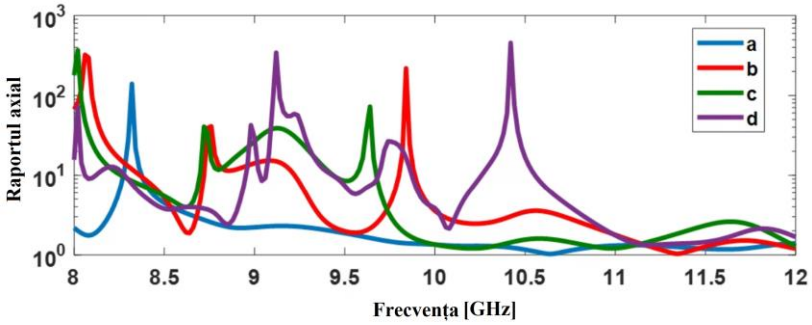

Figure 6.38 *Simulated axial ratio as a function of frequency for $\theta = 0°$ and $\Phi = 0°$*

6.3.4 A calibration procedure for Two-antenna direction of arrival finding systems

By performing a far-field zone calibration in an anechoic chamber a correction factor can be computed and stored in an array:

$$\varepsilon(\varphi, f) = \Delta\Phi(\varphi, f) - k_0 D sin\varphi \tag{6.14}$$

where f is the frequency.

The phase of the transfer factor, S_{21}, is successively measured by connecting the port 1 of the vector analyzer in each antenna, whereas the other antenna is terminated on a load. The resulting correction factor is displayed in Figure 6.44.

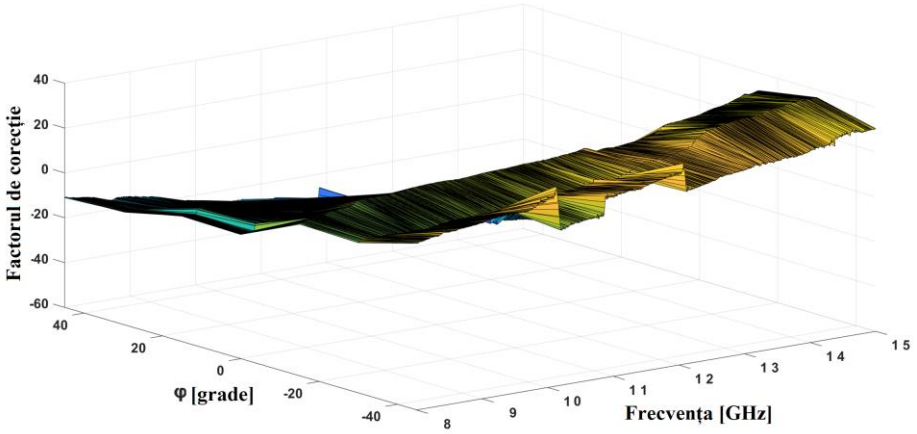

Figure 6.44 *The correction factor*

Chapter 7

Conclusion

In this work, a method for obtaining circular polarization was presented by attaching a structure made of multiple layers of frequency selective surfaces to the aperture of a pyramidal horn antenna. The position of the FSS structures relative to the horn aperture was chosen by analogy with the Yagi-Uda arrays. The presented theoretical foundation allows to explain how the linear polarization of the pyramidal horn type antenna is transformed into circular polarization. Several frequency selective surface structures with different radiator shapes and different numbers of successive layers were analyzed.

Simulations and experimental results show that such a solution leads to a circular polarization with an axial ratio very close to unity at a frequency of 12 GHz, while also obtaining an increase in gain of about 3 dB compared to a conventional antenna horn.

The adopted solution, which can be applied to any conventional horn antenna, has the advantage of a much lower cost compared to the approaches in the specialized literature that assume the creation of dedicated excitation structures in the waveguide.

7.1 Results

In this PhD work, two major directions for obtaining circular polarization with a pyramidal horn antenna were analyzed: by introducing a phase shifter in the excitation guide, respectively by placing a multilayer frequency selective surface in the antenna aperture.

In chapter 5, a technique for obtaining circular polarization was presented consisting of the interposition between the horn antenna and the excitation guide of a slot. At the resonant frequency, the gain is 20 dB.

The sixth chapter is dedicated to the transformation of the polarization of a pyramidal horn antenna by introducing some multiple layers of the frequency selective surfaces into the antenna aperture. The frequency selective surface has been optimized both in terms of the shape of the radiators and the number of successive layers. Following the simulations and experimental determinations carried out on a number of ten configurations, an optimal structure in terms of axial ratio, gain and frequency band resulted. This structure consists of four layers with 4×4 linear radiators in $\lambda/2$ and provides an almost constant axial ratio equal to unity between 11 GHz and 12 GHz and good impedance matching over the entire frequency band of interest. The gain of the radiating system has increased by 3 dB compared to the conventional pyramidal horn antenna. The major advantage of the proposed radiating system with FSS in the horn aperture is the manufacturing cost, since a conventional, general-purpose antenna can be easily converted into a CP antenna with FSS printed on a single-layer metal substrate.

7.2 Original contributions

1. Multi-criteria optimization of a conventional Ku-band pyramidal horn antenna in terms of gain, bandwidth and impedance matching: [LO3], [LO4], the paragraphs 2.5.1 and 2.5.2 from the thesis.
2. Optimizing a Ku-band double ridged guide horn antenna to improve the shape of the radiation pattern in the upper frequency band: [LO1], Chapter 3 from the thesis.
3. Improvement of the method of obtaining circular polarization consisting in the introduction of a slot in the excitation guide: [LO2], Chapter 5 from the thesis.
4. Development and theoretical substantiation of a new method for obtaining circular polarization based on linear radiators: [LO6], the paragraph 6.2.1 from the thesis.
5. Optimizing the shape of linear resonators in order to obtain circular polarization, from the point of view of the phase shift between the orthogonal components of the electric field: [LO6], the paragraph 6.2.2 from the thesis.
6. Designing a new multilayer frequency selective surfaces configuration in which the spacing between successive layers is based on the principle of a Yagi-Uda antenna array: [LO6], the paragraph 6.3.2.2 from the thesis.
7. Optimization of multilayer frequency selective surfaces in terms of the number of layers and the number of radiators in each layer: [LO6], the paragraph 6.3.2 from the thesis.
8. Conception, realization, theoretical and experimental validation of an innovative pyramid horn antenna structure with circular polarization having multilayer frequency selective surfaces in the aperture: [LO6], the paragraphs 6.3.2 and 6.3.3 from the thesis.
9. Conception, realization, theoretical and experimental validation of an assembly of two horn antennas with applications in locating a source of electromagnetic radiation: [LO5], [LO7], the paragraphs 2.5.3 and 6.3.4 from the thesis.
10. Designing a method for calibrating a system of two horn antennas with frequency selective surfaces in the aperture in order to compensate for the effects of mutual coupling and distortion of radiation patterns, with applications in locating a source of electromagnetic radiation: [LO7], the paragraph 6.3.4 from the thesis.

7.3 Publications

[LO1] **A. Heiman**, A. Badescu, *A Novel Design and Simulation of a Ku Broadband Double Ridged Guide Horn Antenna for Satellite Communications*, **in Proceedings of the PhotonIcs & Electromagnetics Research Symposium - Spring**, Roma, Italy, pp. 923-929, doi: 10.1109/PIERS-Spring46901.2019.9017369, WOS: 000550769300136, 17-20 June 2019 – ***index WoS and IEEE Explore.***

[LO2] **A. Heiman**, A. Badescu, *Circularly Polarized Pyramidal Horn Antenna for Ku Band*, **in Proceedings of the IEEE International Conference on Wireless for Space and Extreme Environments**, Vicenza, Italy, pp. 45-48, doi: 10.1109/WiSEE44079.2020.9262465, WOS: 000646221000009, 12-14 Oct. 2020 – ***index WoS and IEEE Xplore***.

[LO3] **A. Heiman**, A. Badescu, *Design of a conventional horn antenna for Ku band*, **in Proceedings of the IEEE International Workshop on Antenna Tehnology**, Bucharest, Romania, doi: 10.1109/iWAT48004.2020.1570612766, WOS: 000627803200028, 25-28 Feb. 2020 – ***index WoS and IEEE Explore.***

[LO4] **A. Heiman**, A. Badescu, *Analysis of Pyramidal Horn Antenna for Ku Band Applications*, **in Proceedings of the International Symposium on Antennas and Propagation**, Taipei, Taiwan, doi: 10.23919/ISAP47258.2021.9614429, 19-22 Oct. 2021 – ***IEEE Explore.***

[LO5] **A. Heiman**, *A Horn Antenna Array Design for the Ku Band*, **in Proceedings of the International Symposium on Electronics and Telecommunications**, Timisoara, Romania, doi: 10.1109/ISETC56213.2022.10009942, 10-11 Nov. 2022 – ***index IEEE Explore and WOS.***

[LO6] **A. Heiman**, R.D. Tamas, *Transforming Linear to Circular Polarization on Horn Antennas by Using Multiple-Layer Frequency Selective Surfaces,* **Sensors**, vol.22. no. 20, doi: 10.3390/s22207838, WOS: 000873439600001, Oct. 2022 – ***index WoS, Q1.***

[LO7] **A. Heiman**, R.D. Tamas, *Calibration procedure for two-antenna direction of arrival syst ems,* **in Proceedings of the IEEE International Workshop on Antenna Tehnology**, 2023 – ***in dex WoS and IEEE Explore; submitted for publication.***

Other published works in the domain

[C1] **Cristina-Adelaida Heiman**, Alina-Mihaela Badescu, *Antenna and Propagation. Laboratory guidebook*, MATRIX ROM, 2020 (ISBN: 978-606-25-0595-0)

[C2] **A. Heiman**, A. Badescu, A. Saftoiu, *A new Multiple Input Multiple Output V2V automotive antenna for Long Term Evolution band applications,* **in Proceedings of the International Symposium on Fundamentals of Electrical Engineering,** Bucuresti, Romania, doi: 10.1109/ISFEE.2018.8742480, WOS: 000480396400073, 01-03 Nov. 2018 – ***index WoS and IEEE Explore***

[C3] D. Tomescu, **A. Heiman**, A. Badescu, *An Automatic Remote Monitoring System for Large Networks,* **in Proceedings of the IEEE International Conference on Computational Science and Engineering (CSE) and IEEE International Conference on Embedded and Ubiquitous Computing (EUC),** New York, USA, pp. 71-73, doi: 10.1109/CSE/EUC.2019.00023, WOS: 000521797300014, 01-03 Aug. 2019 – ***index WoS and IEEE Explore***

7.4 Future research areas

The array of two pyramidal horn antennas with multilayer frequency selective surfaces proposed in this work, intended for the localization of an electromagnetic radiation source, can be improved by studying the mutual coupling effect between the multilayer FSS structures located in the apertures of the two antennas.

Following such a study, passive elements can be designed and made to ensure the reduction of mutual coupling. Also, the calibration operation proposed in this work can be improved by using a guide-coaxial cable transition for both antennas, and the localization accuracy will be able to be evaluated by tracking a real source of electromagnetic radiation located at a great distance (for example, a satellite).

Bibliography

[1] C. A. Balanis, *Antenna Theory, Analysis And Design*, John Wiley, 2016.

[2] M. Abbas-Azimi, F. Arazm și J. Rashed-Mohassel, *Design of a New Broadband EMC Double Ridged Guide Horn Antenna*, în EuCAP, Nice, 2006.

[3] F. Stevenson, *Theory of slots in rectangular waveguides*, Journal of Applied Physics, vol. 19, pp. 24-38, 1948.

[4] R. S. Elliot, *Antenna theory & design*, Canada: IEEE Press Series on Electromagnetic wave theory, 2003.

[5] L. J. Wang, X. Gao și F. L. Yu, *A compact and broadband circularly polarized horn antenna*, Chengdu, 2018.

[6] A. E. Farahat și K. F. A. Hussein, *Spatial Filters for Linearly Polarized Antennas Using Free Standing Frequency Selective Surfaces*, Electromagnetics Research, vol. 2, pp. 167-188, 2008.

[7] N. Landy, *Perfect Metamaterial Absorber*, Physics Re. Lett., 2008.

[8] D. Pozar, *Microwave Engineering*, John Wiley & Song, 2005.

[9] K. Delihacioglu, *Frequency Selective Surfaces With Multiple-Strip Group Elements*, IEEE Antennas and Wireless Propag. Lett., vol. 11, pp. 1370-1373, 2012.

[10] D. Cure, T. Weller și F. Miranda, *A comparison between Jerusalem Cross and Square Patch Frequency Selective Surfaces for low profile antenna appl*ications, în International Conference on Electromagnetics in Advanced Applications, 2011.

[11] R. Mittra, R. C. Hall și T. Chich-Hsing, *Spectral-domain analysis of circular patch frequency selective surfaces*, IEEE Transactions on Antennas and Propagation, vol. 32, pp. 533-536, 1984.

[12] L. Bin, B. Ming, M. Hui, Z. Haibo și M. Jungang, *Four-band frequency selective surface with circular ring patch elements*, în International Conference on Microwave and Milimeter Wave Technology, 2012.

[13] W. Te-Kao, *Four-band frequency selective surface with double-square-loop patch elements*, IEEE Trans. on Antennas and Propag., vol.42, pp. 1659-1663, 1994.

[14] H. U. Tahseen, L. Yang și X. Zhou, *Design of FSS-antenna-radome system for airborne and ground applications*, IET Commun., vol. 5, pp. 1691-1699, 2021.

[15] J. Y. Yin, X. Wan, J. Ren și T. J. Cui, *A Circular Polarizer with Beamforming Feature Based on Frequency Selective Surfaces*, Sci. Rep., vol. 7, pp. 1-10, 2017.

[16] C. Yang, X. W. Zhu, P. Liu, W. Hong, H. Feng și Y. Shi, *A Circularly Polarized Horn Antenna Based on FSS Polarization Converter*, IEEE Antenna Wirel. Propag. Lett., vol. 19, nr. 2, pp. 277-281, 2019.